Article

Cell Reports

Blunted mGluR Activation Disinhibits Striatopallidal Transmission in Parkinsonian Mice

Graphical Abstract

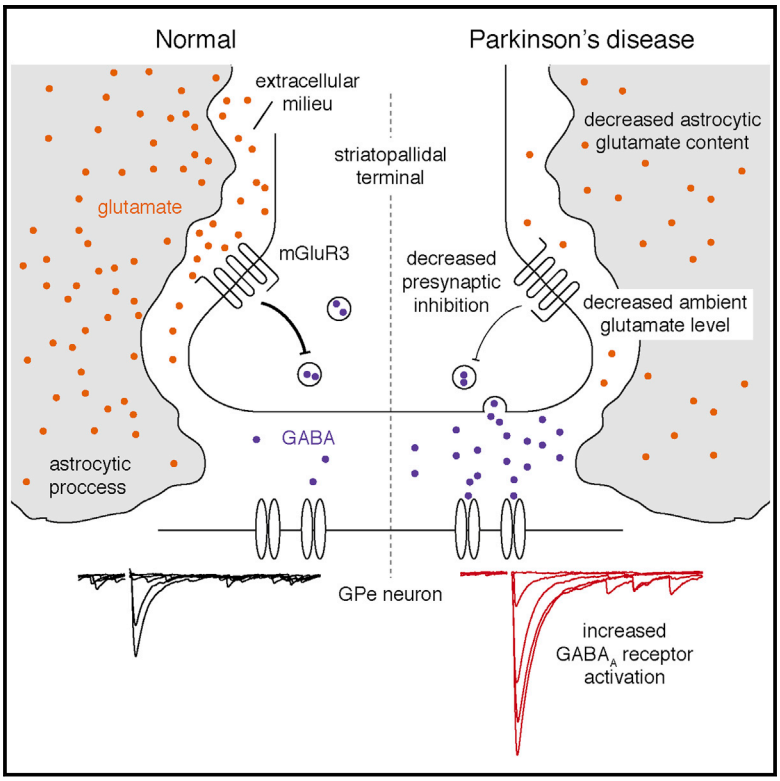

Highlights

- An ambient level of glutamate is maintained in the GPe ex vivo
- GPe astrocytes gate striatopallidal transmission via presynaptic group II mGluRs
- GPe astrocytes display altered glutamate homeostasis in models of PD
- Reduced mGluR activation leads to overactive striatopallidal transmission in PD

Authors

Qiaoling Cui, Jason E. Pitt, Arin Pamukcu, ..., Robert T. Kennedy, Rajeshwar Awatramani, C. Savio Chan

Correspondence

saviochan@gmail.com

In Brief

In Parkinson's disease, the overactivity of the striatopallidal pathway is thought to underlie hypokinetic symptoms. In this study, Cui et al. demonstrate that astrocytes local to the pallidum play a crucial role in controlling the gain of striatopallidal transmission. This regulatory process goes awry after a chronic loss of dopamine.

Cui et al., 2016, Cell Reports *17*, 2431–2444
November 22, 2016
http://dx.doi.org/10.1016/j.celrep.2016.10.087

Cell Reports
Article

Blunted mGluR Activation Disinhibits Striatopallidal Transmission in Parkinsonian Mice

Qiaoling Cui,[1] Jason E. Pitt,[1] Arin Pamukcu,[1] Jean-Francois Poulin,[2] Omar S. Mabrouk,[3] Michael P. Fiske,[1] Isabel B. Fan,[1] Elizabeth C. Augustine,[1] Katherine A. Young,[1] Robert T. Kennedy,[3] Rajeshwar Awatramani,[2] and C. Savio Chan[1,4,*]
[1]Department of Physiology, Feinberg School of Medicine, Northwestern University, Chicago, IL 60611, USA
[2]Department of Neurology, Feinberg School of Medicine, Northwestern University, Chicago, IL 60611, USA
[3]Department of Pharmacology, University of Michigan Medical School, Ann Arbor, MI 48109, USA
[4]Lead Contact
*Correspondence: saviochan@gmail.com
http://dx.doi.org/10.1016/j.celrep.2016.10.087

SUMMARY

The prevailing circuit model predicts that hyperactivity of the striatopallidal pathway and subsequently increased inhibition of external globus pallidus (GPe) neurons lead to the hypokinetic symptoms of Parkinson's disease (PD). It is believed that hyperactivity of the striatopallidal pathway is due to inactivity of dopamine receptors on the somatodendritic membrane of striatopallidal neurons, but the exact cellular underpinnings remain unclear. In this study, we show that mouse GPe astrocytes critically control ambient glutamate level, which in turn gates striatopallidal transmission via the activation of presynaptic metabotropic glutamate receptors. This presynaptic inhibition of striatopallidal transmission is diminished after the chronic loss of dopamine. Elevation of intracellular glutamate content in astrocytes restores the proper regulation of the striatopallidal input in PD models. These findings argue that astrocytes are key regulators of the striatopallidal synapse. Targeting this cell class may serve as an alternative therapeutic strategy for PD.

INTRODUCTION

Astrocytes are integral elements of neural circuits. Through the expression of a myriad of surface receptors, astrocytes integrate local and long-range modulatory signals and interact with neurons through the transport and release of neuroactive substrates (Araque et al., 2014; Halassa et al., 2007; Perea et al., 2009; Theodosis et al., 2008). As our understanding of the role of astrocytes emerged from only a few selected brain areas, we are just beginning to appreciate the biological importance and disease relevance of astrocytes in the basal ganglia (Martín et al., 2015; Tong et al., 2014).

Previous studies suggest astrocytes are enriched in the external globus pallidus (GPe) of the basal ganglia (Lange et al., 1976; Salvesen et al., 2015). This abundance implies that astrocytes may play a crucial role in regulating GPe function. Ultrastructural studies suggest that GPe astrocytic processes are juxtaposed to striatopallidal terminals and are thus poised to regulate striatopallidal synaptic transmission (Galvan et al., 2010). While GPe astrocytes are likely vital in supporting striatopallidal transmission via the clearance and recycling of important substrates, it is unclear whether they actively control striatopallidal transmission. Furthermore, we do not know if these processes are under the influence of dopamine, which is lost in Parkinson's disease (PD) (Hornykiewicz, 1998; Wichmann and DeLong, 1996). Since hyperactive striatopallidal signaling is thought to underlie hypokinetic symptoms of PD (Kravitz et al., 2010; Lemos et al., 2016), we sought to determine if disruption of astrocytic regulation could account for this altered circuit behavior in PD.

RESULTS

GPe Astrocytes Are Regulated by Dopamine

In keeping with the previous findings of astrocyte enrichment in the GPe, high levels of GFAP (an astrocytic marker) were observed in this brain area (Figure 1A; Figure S1). To confirm the enrichment of astrocytes, neuron and astrocyte abundance in the GPe was estimated. Accordingly, a $Gfap^{Cre}$ mouse line was used to target a broad range of GPe astrocytes. As expected, *Cre*-inducible tdTomato expression colocalized with the astrocyte-specific markers GFAP, Aldh1l1, and S100β (Figure 1B; Figure S1). Consistent with earlier observations, quantitative analysis of astrocyte ($tdTomato^+$) and neuron ($NeuN^+$) abundance revealed an enrichment of astrocytes in the GPe. The astrocyte-to-neuron ratio was an order of magnitude higher in the GPe than in the dorsal striatum (dStr) (GPe = 1.8 ± 0.4, dStr = 0.13 ± 0.03; $p < 0.0001$) (Figure 1B; Table S1). A similar difference in the astrocyte-to-neuron ratio between the GPe and the dStr was obtained using S100β as the marker for astrocytes (GPe = 0.88 ± 0.21, dStr = 0.17 ± 0.04; $p < 0.0001$).

Astrocytes exhibit spontaneous calcium (Ca^{2+}) transients, which have important implications in a variety of neural circuits and provide a useful measure of their physiology (Agulhon et al., 2008; Bazargani and Attwell, 2016; Khakh and Sofroniew, 2015; Nedergaard et al., 2010; Perea and Araque, 2005; Shigetomi et al., 2016). To monitor spontaneous Ca^{2+} transients in GPe astrocytes, the expression of a cytosolic Ca^{2+} sensor was accomplished with a genetic cross using the same $Gfap^{Cre}$ mouse line with a *Cre*-inducible GCaMP3 mouse line. Similar

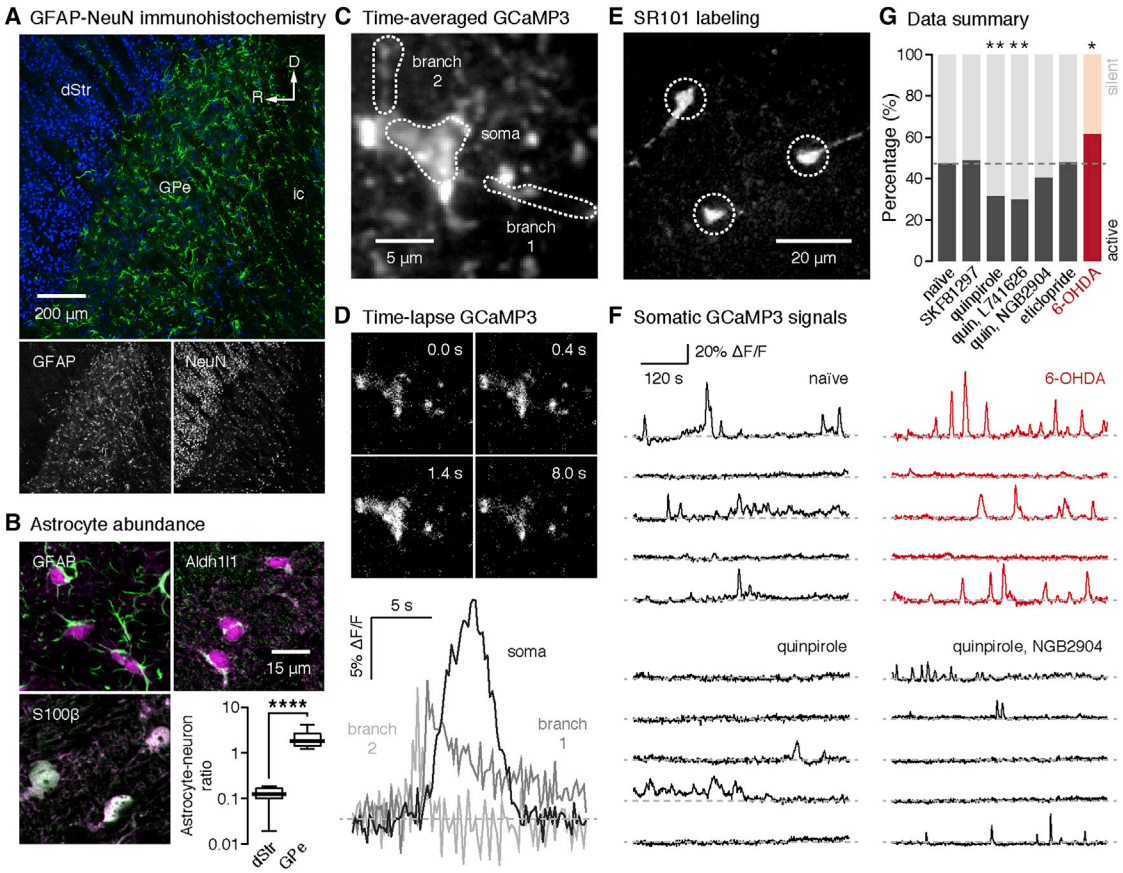

Figure 1. The GPe Harbors a High Abundance of Astrocytes that Are Regulated by Dopamine

(A) Confocal micrograph of an adult mouse brain section showing GFAP (green) and NeuN (blue) immunoreactivity in the external globus pallidus (GPe) and the dorsal striatum (dStr). The two channels are also separated and presented in grayscale. ic, internal capsule.

(B) $Gfap^{Cre}$ driver line was crossed with a $R26^{LSL\text{-}tdTomato}$ reporter line ($Gfap^{Cre}$;$R26^{LSL\text{-}tdTomato}$) to genetically label astrocytes (magenta) in the GPe. The specificity of *Cre-lox*-mediated recombination events was demonstrated by the colocalization of tdTomato signal (magenta) with three different astrocyte-specific markers (green), GFAP, Aldh1l1, and S100β. Boxplots summarized the astrocyte-to-neuron ratios in the dStr and GPe. Density (1,000 cells × mm^{-3}) of genetically labeled astrocytes (GPe, n = 30 z stacks; dStr, n = 30 z stacks; $p < 0.0001$) and immunolabeled neuron cell bodies (GPe, n = 30 z stacks; dStr, n = 30 z stacks; $p < 0.0001$) were quantified. The astrocyte-neuron ratio was different between the GPe and the dStr (GPe, n = 30 z stacks; dStr, n = 30 z stacks; $p < 0.0001$). Astrocytic abundance in the GPe was quantified in two $Gfap^{Cre}$;$R26^{LSL\text{-}tdTomato}$ mice. Whiskers of the boxplots represent 10–90th percentiles.

(C) A confocal image shows the time-averaged GCaMP3 signals in a GPe astrocyte from a $Gfap^{Cre}$;$R26^{LSL\text{-}GCaMP3}$ mouse.

(D) Top: a series of time-lapse images showing compartment-specific dynamics of GCaMP3 signals. Bottom: Ca^{2+} transients measured in soma and two different branches are shown.

(E) SR101 was used to define regions of interest (ROIs). A representative spinning-disk confocal image shows SR101-labeled GPe astrocytes.

(F) Representative somatic GCaMP3 signals from GPe astrocytes in different conditions. Five individual GPe astrocytes are shown in each condition.

(G) Stacked bar graph summarizing the percentage of GPe astrocytes that displayed somatic GCaMP3 signals (black or red, active) and those that did not (gray or pink, silent) in different conditions (naive, n = 413 cells; SKF 81297, n = 109 cells; quinpirole, n = 140 cells; quinpirole and L741626, n = 104 cells; quinpirole and NGB 2904, n = 123 cells; eticlopride, n = 260 cells; 6-OHDA, n = 91 cells). Dopamine D1 class receptor agonist SKF 81297 did not change the percentage of active GPe astrocytes compared to the drug-free controls in naive mice ($p = 0.7934$). Dopamine D2 class receptor agonist quinpirole reduced the percentage of active astrocytes ($p = 0.0011$). Co-application of quinpirole and a D2 receptor antagonist L741626 did not block the effect of quinpirole ($p = 0.0091$). Co-application of quinpirole with a D3 receptor antagonist NGB 2904 blocked the effect of quinpirole ($p = 0.9181$). D2 class receptor antagonist eticlopride did not change the percentage of active GPe astrocytes ($p = 0.0946$). Chronic 6-OHDA lesion increased the percentage of active astrocytes compared to naive mice ($p = 0.0133$). All statistical analyses compared between drug applications or chronic 6-OHDA lesion with drug-free controls in naive mice.

to those observed in prototypical astrocytes, GPe astrocytes displayed somatic Ca^{2+} transients, spreading waves, and compartment-specific Ca^{2+} dynamics (Figures 1C and 1D). Somatic Ca^{2+} transients were measured in the subsequent analyses because of their robustness in detection. Accordingly, SR101 was used for unbiased identification of the GPe astrocytes' cell body (Figure 1E) (Nimmerjahn et al., 2004). Spontaneous somatic Ca^{2+} transients were observed in 47.2% of the astrocyte cell bodies (n = 413 cells) during a 10-min imaging block (Figures 1F and 1G; Figure S2).

To investigate if GPe astrocytes are under the influence of dopamine, the effects of bath-applied dopamine receptor

ligands on spontaneous Ca^{2+} transients were examined. Activation of D2 class dopamine receptors by quinpirole (10 μM) reduced the percentage of naive GPe astrocytes that displayed spontaneous Ca^{2+} transients when compared to astrocytes in drug-free imaging fields or slices (see the Supplemental Experimental Procedures) (31.4%, n = 140 cells; p = 0.0011) (Figures 1F and 1G). This effect was not due to collateral changes in the GPe neurons' firing, as quinpirole had no consistent effect on their firing (Figure S2). Quinpirole-induced suppression of astrocytic spontaneous Ca^{2+} transients was blocked with NGB2904 (50 nM), a D3 receptor-specific antagonist (48.0%, n = 123 cells; p = 0.9181) (Figures 1F and 1G), but not with L741626 (10 nM), a D2 receptor-specific antagonist (29.8%, n = 104 cells; p = 0.0091) (Figure 1G; Figure S2). Antagonism of D2 class dopamine receptors by eticlopride (100 nM) did not alter the percentage of naive GPe astrocytes that displayed spontaneous Ca^{2+} transients (40.4%, n = 260 cells; p = 0.0946) (Figure 1G; Figure S2). Similarly, activation of D1 class receptors by SKF 81297 (5 μM) had no effect on the percentage of active GPe astrocytes (48.6%, n = 109 cells; p = 0.7934) (Figure 1G; Figure S2). The duration and amplitude of somatic Ca^{2+} transients were not different with pharmacological treatments (Figure S2).

Given astrocyte sensitivity to dopamine receptor modulation, we next examined if GPe astrocytes are affected by chronic 6-OHDA lesion, which results in extensive dopamine cell loss in the midbrain, as seen in PD. Spontaneous Ca^{2+} transients were observed in a higher percentage of the astrocyte cell bodies following chronic 6-OHDA lesion when compared to GPe astrocytes from naive mice (61.5%, n = 91 cells; p = 0.0133). Additionally, increases in both frequency and amplitude of spontaneous Ca^{2+} transients in GPe astrocytes were observed under the same experimental conditions (Figures 1F and 1G; Figure S2). However, these changes were not the consequence of GPe astrocyte reactivity, as their abundance and morphological properties were unaltered following chronic 6-OHDA lesion (Figure S1).

An Ambient Glutamate Level Is Maintained in the GPe Ex Vivo

While our data suggest that GPe astrocytes are under the influence of dopamine, the exact function of GPe astrocytes remains to be determined. A prominent feature of GPe astrocytes is their high expression level of GFAP (Figure 1A; Figure S1). One of the critical roles of GFAP is the regulation of astrocytic glutamate transporters (Middeldorp and Hol, 2011). Consistent with this notion, immunoreactivity for EAAT1 and EAAT2 (also known as GLAST and GLT1, respectively) was observed throughout the GPe (Figure S3). We hypothesized that GPe astrocytes are involved in the maintenance of glutamate homeostasis.

Early kinetic modeling suggests that glutamate transporters display transport and unbinding of glutamate with equal probability. In other words, in addition to rapid sequestration of glutamate, astrocytic glutamate transporters can also maintain an ambient level of glutamate in the extracellular milieu if provided with a constant source of glutamate (Tzingounis and Wadiche, 2007). To examine such a possibility, we investigated the glutamate content in the GPe in ex vivo slices by expressing a genetically encoded glutamate sensor iGluSnFR (Marvin et al., 2013) on GPe astrocytes. As predicted, exogenously applied glutamate dose-dependently increased iGluSnFR signals in ex vivo GPe tissue (Figure 2A). Glutamate at 10 μM reliably increased iGluSnFR signals by ~10% (1.129 ± 0.052-fold; p < 0.0001). On the other hand, bath application of NBQX (100 μM, which acts as a non-specific fluorescence quencher) decreased basal iGluSnFR signals in ex vivo GPe tissue (0.862 ± 0.021-fold; p < 0.0001). Parallel analysis in the dStr resulted in a more modest decrease in basal iGluSnFR signals (0.930 ± 0.030-fold; p < 0.0001) (Figure 2B). These data argue that a higher level of ambient glutamate was present in the GPe than in the dStr ex vivo (p = 0.0122). Given that iGluSnFR displays an affinity for glutamate similar to that of NMDA receptors (Dingledine et al., 1999; Featherstone and Shippy, 2008; Marvin et al., 2013; Traynelis et al., 2010), one should expect tonic NMDA receptor activity in GPe neurons. Consistent with our hypothesis, whole-cell voltage-clamp recordings from GPe neurons in the presence of tetrodotoxin (TTX, 1 μM) uncovered that NMDA receptors in ex vivo GPe tissue were tonically active (Figures 2C–2E).

Ambient Glutamate Gates Striatopallidal GABA Transmission through Group II mGluR Activation

Previous ultrastructural studies show astrocytic processes are juxtaposed to the GABAergic striatopallidal terminals (Galvan et al., 2010). As astrocytic glutamate transporters are present at GABAergic synapses (Benediktsson et al., 2012; Minelli et al., 2001), it is plausible that GPe astrocytes control striatopallidal transmission by regulating the ambient glutamate that acts on presynaptic group II metabotropic glutamate receptors (mGluRs) (Kalivas, 2009). While mGluR2 (one of the two members of group II mGluRs) is not expressed in striatal projection neurons (SPNs) (Testa et al., 1994), cell-specific expression analysis showed that mGluR3 is expressed in both direct and indirect pathway SPNs (Figure S4). These data are in agreement with prior observations showing robust mGluR3 in striatal tissue (Ohishi et al., 1993; Tanabe et al., 1993; Testa et al., 1994). Therefore, we hypothesize that GPe astrocytes control striatopallidal signaling by regulating the availability of glutamate to mGluR3.

To demonstrate the functional expression of mGluR3 at the striatopallidal terminals, the effect of group II mGluR activation on striatopallidal GABA release was examined. Bath application of a selective group II mGluR agonist LY379268 (100 nM) reduced (0.5 ± 0.2-fold; p = 0.002) the amplitude of evoked inhibitory postsynaptic currents (eIPSCs) with a concomitant increase in their coefficient of variation ([CV] an indicator of a locus of synaptic modulation) (Del Castillo and Katz, 1954; Malinow and Tsien, 1990) (control = 0.60 ± 0.13, LY379268 = 0.96 ± 0.34; p = 0.0039) (Figures 3A and 3B). Consistent with this observation, LY379268 decreased maximal peak amplitude (LY379268 = 0.8 ± 0.2-fold; n = 6 cells; p = 0.0313) and quantal event frequency (control = 22.7 ± 6.0 Hz, LY379268 = 15.5 ± 5.1 Hz; n = 6 cells; p = 0.0313), but not quantal IPSC amplitude (control = 60.3 ± 4.2 pA, LY379268 = 64.8 ± 5.3 pA; n = 6 cells; p = 1.0000) in strontium (Sr^{2+})-containing external solution, which provided a different metric for estimation of release (Figure S5). These data are in agreement with our

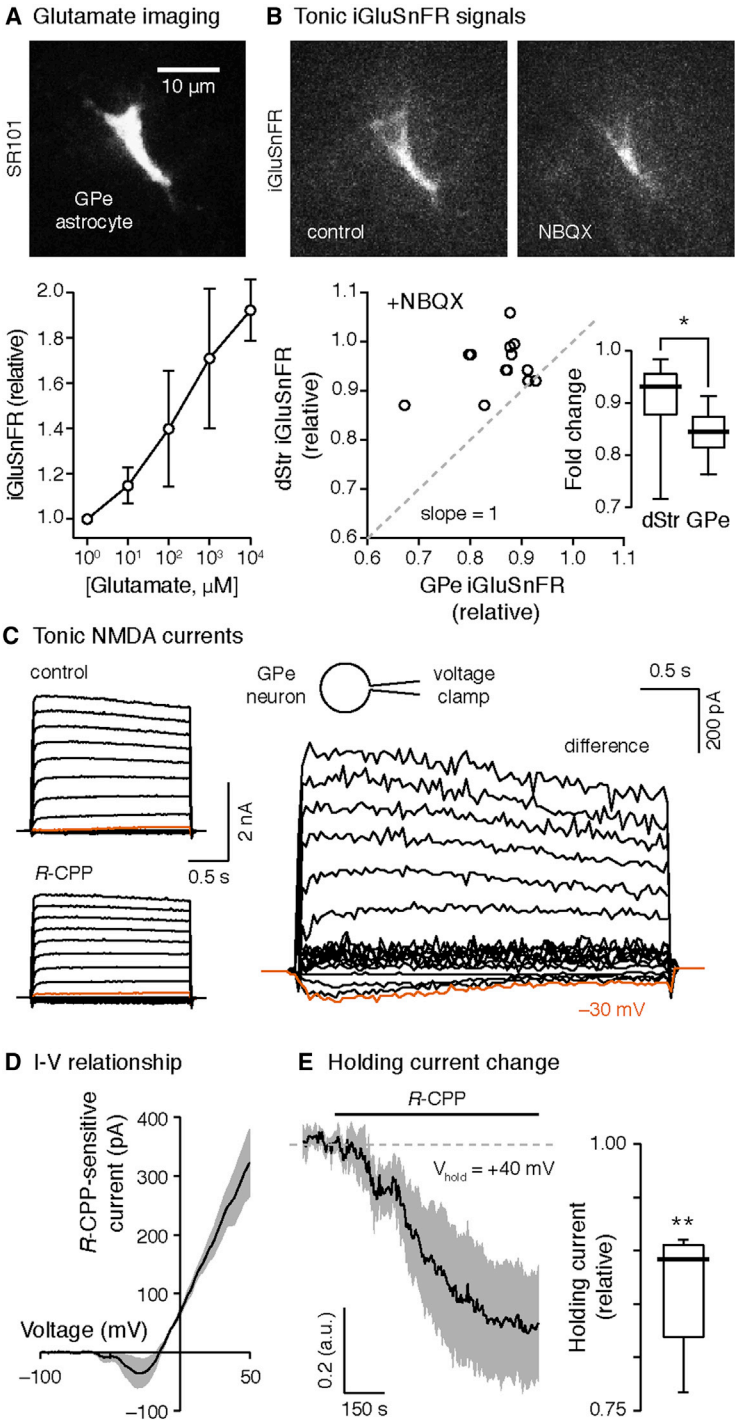

Figure 2. Tonic Activation of iGluSnFR and NMDA Receptors in the GPe

(A) Top: a confocal micrograph showing a GPe astrocyte labeled with SR101. Bottom: dose response of iGluSnFR to exogenously applied glutamate (10^0–10^4 μM) is shown. Means ± SEMs are presented.

(B) Top: basal iGluSnFR signal (left) in the GPe was attenuated by the application of NBQX (100 μM, right). Bottom: the correlated changes in iGluSnFR signal with NBQX in the dStr and the GPe from single mice are shown. The no-effect line (dotted line) has a slope = 1. Inset: boxplots show a larger reduction in iGluSnFR signal in the GPe than in the dStr (GPe, n = 23 slices; dStr, n = 15 slices; p = 0.0122).

(C) Current-voltage relationship of tonic NMDA currents in GPe neurons, assessed using voltage steps from –120 mV to +70 mV with 10-mV increments, is shown.

(D) Current-voltage relationship of tonic NMDA currents in GPe neurons, assessed using a voltage-ramp protocol, is shown.

(E) Left: tonic NMDA currents were revealed by *R*-CPP (10 μM) application in GPe neurons that were held at +40 mV. Right: boxplots summarize the effect of *R*-CPP on holding currents in GPe neurons (n = 5 cells, p = 0.0072). A one-sample t test was used to compare the relative change in holding current after *R*-CPP. TTX (1 μM) was included in the perfusate in (C)–(E). Whiskers of the boxplots represent 10–90th percentiles.

hypothesis that group II mGluRs are localized presynaptically on the striatopallidal terminals.

As we observed that ambient glutamate was present at a concentration sufficient to activate iGluSnFR and NMDA receptors in ex vivo GPe tissue, we examined if ambient glutamate tonically activates presynaptic group II mGluRs. LY341495 (200 nM, an antagonist for group II mGluRs) (Schoepp et al., 1999) increased (2.3 ± 0.9-fold; p = 0.002) the amplitude of striatopallidal eIPSCs (Figures 3A and 3B). This increase was accompanied by a reduction in the CV of eIPSCs (control = 0.60 ± 0.17, LY341495 = 0.26 ± 0.07; p = 0.002) (Figure 3A). Sequential LY379268 and LY341495 applications estimated a high level (73.0% ± 19.6%) of receptor activity in ex vivo slices (Figure 3C). The increase in striatopallidal GABA release with group II mGluR antagonism was also observed in Sr^{2+}-containing external solution (Figure S5).

The effects produced by LY341495 suggest that a receptor tone was maintained in the ex vivo slice. To assert the selective involvement of group II mGluRs, the effect of MNI-137, a group II mGluR negative allosteric modulator (NAM), was examined. MNI-137 (2 μM) produced an increase (2.6 ± 0.8-fold; p = 0.0313) in striatopallidal eIPSC amplitude with a reduction in eIPSC CV (control = 0.51 ± 0.18, MNI-137 = 0.30 ± 0.16; p = 0.0156). The impact of MNI-137 on eIPSC amplitude was indistinguishable from that of LY341495 (p = 0.8452) (Figures 3A and 3B). As a NAM, MNI-137 should, in theory, be inactive in the absence of the orthosteric ligand (i.e., glutamate). The effects produced by MNI-137 indicated that the tonic activity of group II mGluRs at the striatopallidal synapse was maintained by glutamate in the ex vivo GPe tissue, corroborating the inference drawn from our measurements with iGluSnFR and NMDA receptors.

Lastly, to demonstrate LY341495 did not act directly on GPe astrocytes, astrocyte spontaneous Ca^{2+} transients were used as a readout. LY341495 application did not affect the percentage of naive GPe astrocytes that displayed spontaneous Ca^{2+} transients and does not provide support for the presence of mGluR3

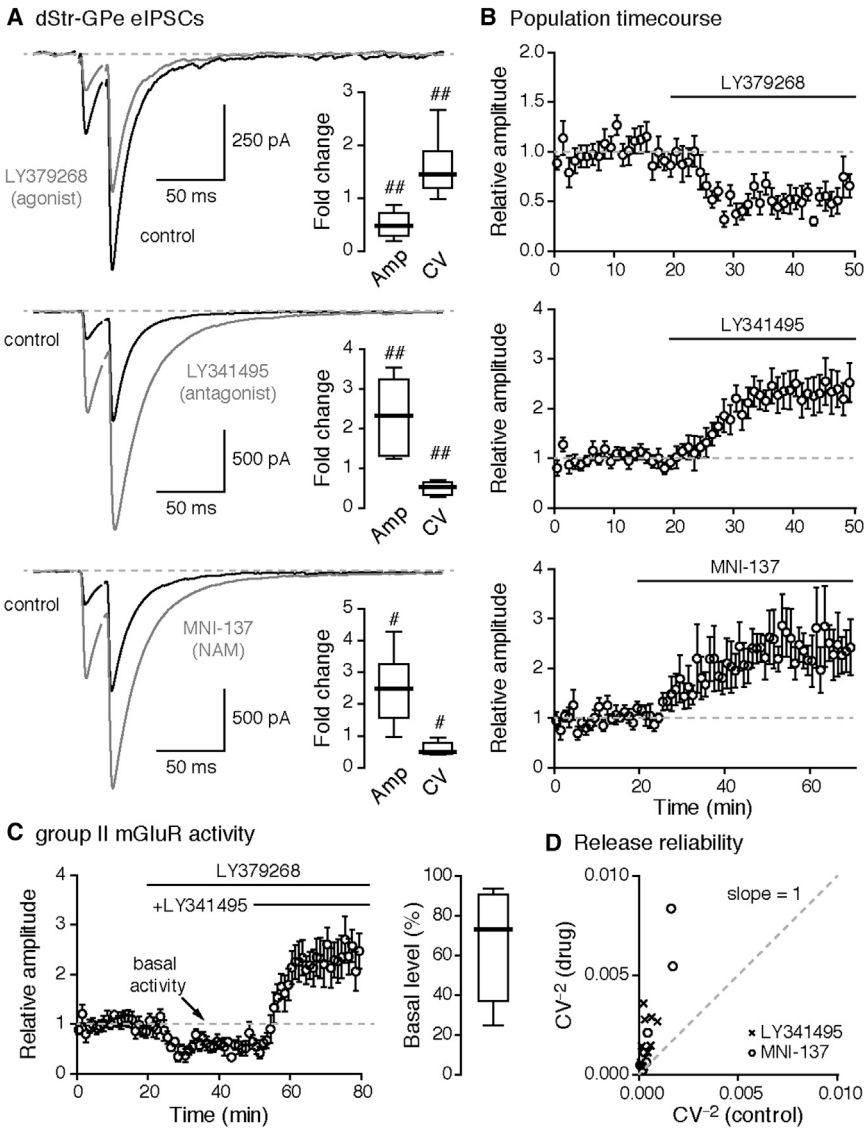

Figure 3. Tonic Group II mGluR Activation Regulates dStr-GPe GABA Release

(A) Top: representative recordings showing a suppression of striatopallidal (dStr-GPe) evoked inhibitory postsynaptic currents (eIPSCs) by LY379268 (100 nM), a group II mGluR agonist. Inset: boxplots summarize the effect of LY379268 on eIPSC amplitude (n = 10 cells, p = 0.002) and CV (n = 10 cells, p = 0.0039). Middle: representative dStr-GPe eIPSCs show a facilitatory effect by LY341495 (200 nM), a group II mGluR antagonist. Inset: boxplots summarize the effect of LY341495 on eIPSC amplitude (n = 10 cells, p = 0.002) and CV (n = 10 cells, p = 0.002). Bottom: representative dStr-GPe eIPSCs show a facilitatory effect by MNI-137 (2 μM), a group II mGluR negative allosteric modulator. Inset: boxplots summarize the effect of MNI-137 on eIPSC amplitude (n = 7 cells, p = 0.0313) and CV (n = 7 cells, p = 0.0156).

(B) Population time course of LY379268 (top), LY341495 (middle), and MNI-137 (bottom) on dStr-GPe eIPSC amplitude is shown.

(C) Left: the basal activity (dotted line) of group II mGluRs was estimated by maximal receptor agonism and antagonism using LY379268 and LY341495, respectively. The population time course is shown. Right: boxplot summary shows the resting activity of group II mGluRs on a per-cell basis (n = 8 cells).

(D) The reliability of the dStr-GPe synapse was measured with CV^{-2}. LY341495 and MNI-137 caused a similar (p = 0.5362) increase in CV^{-2} (LY341495, n = 10 cells, p = 0.002; MNI-137, n = 7 cells, p = 0.0156).

Whiskers of the boxplots represent 10–90th percentiles. Means ± SEMs are presented for the time course plots.

in GPe astrocytes. In contrast, consistent with the presence of ambient glutamate in the GPe, the application of MTEP (an mGluR5 antagonist, 2 μM) decreased the percentage of naive GPe astrocytes that displayed spontaneous Ca^{2+} transients ex vivo (Figure S2).

Neuronal Glutamatergic Inputs Do Not Contribute to Ambient Glutamate Levels Ex Vivo

As ambient glutamate was present in our ex vivo slice preparation in the presence of TTX (Figures 2C–2E), this suggests a possible non-neuronal origin of glutamate. To further investigate the source of glutamate, the effect of LY341495 on miniature IPSCs (mIPSCs) of GPe neurons was examined in the presence of TTX (1 μM) to block action potential-dependent neurotransmitter release. These mIPSCs were considered to originate largely from striatopallidal synapses (Hegeman et al., 2016; Shink and Smith, 1995). LY341495 increased the mIPSC frequency (control = 6.3 ± 1.1 Hz, LY341495 = 9.7 ± 3.4 Hz; n = 6 cells; p = 0.0313) without changing the mIPSC amplitude (control = 46.6 ± 9.9 pA, LY341495 = 57.6 ± 11.3 pA; n = 6 cells; p = 0.2188), further suggesting a non-neuronal source of ambient glutamate and a presynaptic locus of action.

To selectively suppress neuronal glutamatergic input to the GPe, tetanus toxin light chain (TeTLC)-expressing adeno-associated viruses (AAVs) were injected into the subthalamic nucleus (STN)—the primary neuronal glutamatergic input to the GPe (Hegeman et al., 2016; Jaeger and Kita, 2011) (Figures 4A and 4B). Alternatively, STN output was silenced using a conditional VGluT2 knockout (VGluT2-cKO) approach by injecting AAVs encoding *Cre* recombinase (Cre-AAV) into the STN of floxed-VGluT2 mice. To evaluate the effectiveness of the silencing approaches, their behavioral impact was first examined. Consistent with the circuitry model (Tepper et al., 2007; Albin et al., 1989; DeLong, 1990), suppression of the STN output greatly reduced STN-GPe excitatory postsynaptic current (EPSC) amplitude (control = 135.8 ± 129.4 pA, STN silencing = 12.3 ± 12.3 pA; p = 0.0004) and led to contralateral turning behavior

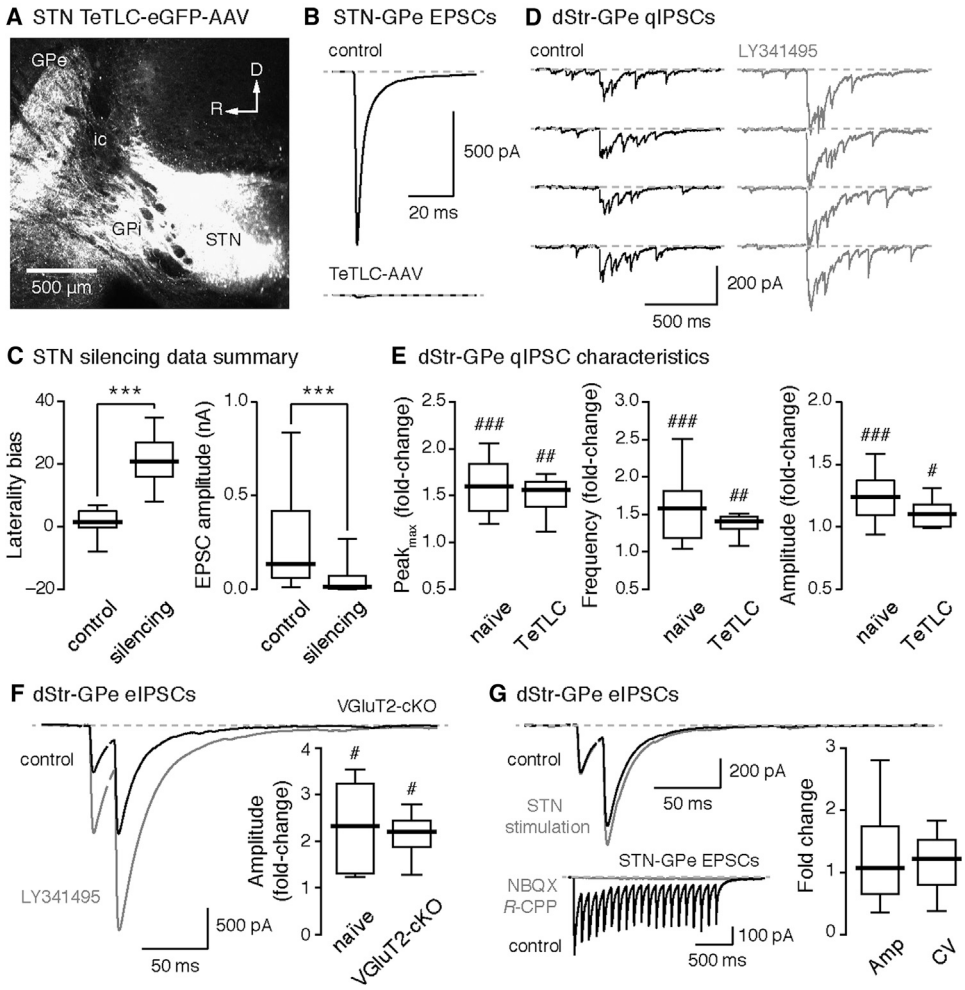

Figure 4. Group II mGluRs Are Targeted by a Non-neuronal Source of Glutamate

(A) A confocal micrograph shows the infection of the subthalamic nucleus (STN) with a tetanus toxin light chain and eGFP-expressing adeno-associated virus (TeTLC-eGFP-AAV). GPi, internal globus pallidus; ic, internal capsule.

(B) Representative recordings showing a near-complete abolishment of STN-GPe excitatory postsynaptic currents (EPSCs) following STN silencing with TeTLC (bottom) compared to control (top). STN-GPe EPSCs were optogenetically evoked.

(C) Left: summarized boxplots showing that rotational behavior toward the side contralateral to the injection was observed in mice with STN silencing by TeTLC-eGFP-AAV or VGluT2-cKO. This behavior is different from that produced with STN injection of an eGFP-expressing AAV (control, n = 14 mice; silencing, n = 19 mice; $p < 0.0001$). Right: boxplots show that STN-GPe EPSC amplitude is largely reduced with STN silencing (n = 19 cells, $p = 0.0004$).

(D) A representative recording demonstrates the effect of LY341495 (200 nM) on dStr-GPe quantal inhibitory postsynaptic currents (qIPSCs) in mice with STN-GPe input suppressed with TeTLC-eGFP-AAV infection.

(E) Summarized boxplots show that LY341495 applications consistently produced comparable effects in maximal peak amplitude, frequency, and quantal amplitude of dStr-GPe qIPSCs (maximal peak: naive, n = 16 cells; TeTLC, n = 8 cells; $p = 0.4440$; frequency: naive, n = 16 cells; TeTLC, n = 8 cells; $p = 0.4440$; quantal amplitude: naive, n = 15 cells; TeTLC, n = 7 cells; $p = 0.1481$) in mice with STN TeTLC-eGFP-AAV infection compared to naive, non-transduced mice.

(F) A representative recording showing the facilitatory effect of LY341495 on dStr-GPe eIPSCs in VGluT2-cKO mice. Inset: no alteration in the effect of LY341495 is observed in VGluT2-cKO mice compared to naive mice (naive, n = 10 cells; VGluT2-cKO, n = 6 cells; $p = 0.9136$).

(G) Top: a representative recording showing the lack of an effect of STN conditioning on dStr-GPe eIPSCs. Bottom: a representative recording in a GPe neuron shows that the STN-conditioning protocol with optogenetic stimulation of STN neurons evoked rapid EPSCs that were temporally synced with the 10-Hz stimulation pulse (n = 13 cells). Glutamatergic nature of the STN-GPe EPSC was pharmacologically confirmed with NBQX (5 µM) and *R*-CPP (20 µM) (n = 3 cells). Inset: boxplot summary shows that neither eIPSC amplitude (STN stimulation, n = 18 cells, $p = 0.5421$) nor CV (STN stimulation, n = 18 cells, $p = 0.2066$) was affected by STN stimulation.

Whiskers of the boxplots represent 10–90th percentiles.

(control = 1.5 ± 2.0 turns, STN silencing = 21.0 ± 5.0 turns; $p < 0.0001$) (Figure 4C). Importantly, we did not observe any alteration in LY341495-induced increase in striatopallidal eIPSCs when STN output was suppressed either with TeTLC (naive = 1.6 ± 0.3-fold, TeTLC = 1.6 ± 0.1-fold; $p = 0.4440$) or with VGluT2-cKO (naive = 2.3 ± 0.9-fold, VGluT2-cKO = 2.2 ± 0.1-fold; $p = 0.9136$) (Figures 4E and 4F). Finally, we tested whether direct stimulation of the STN input could activate group

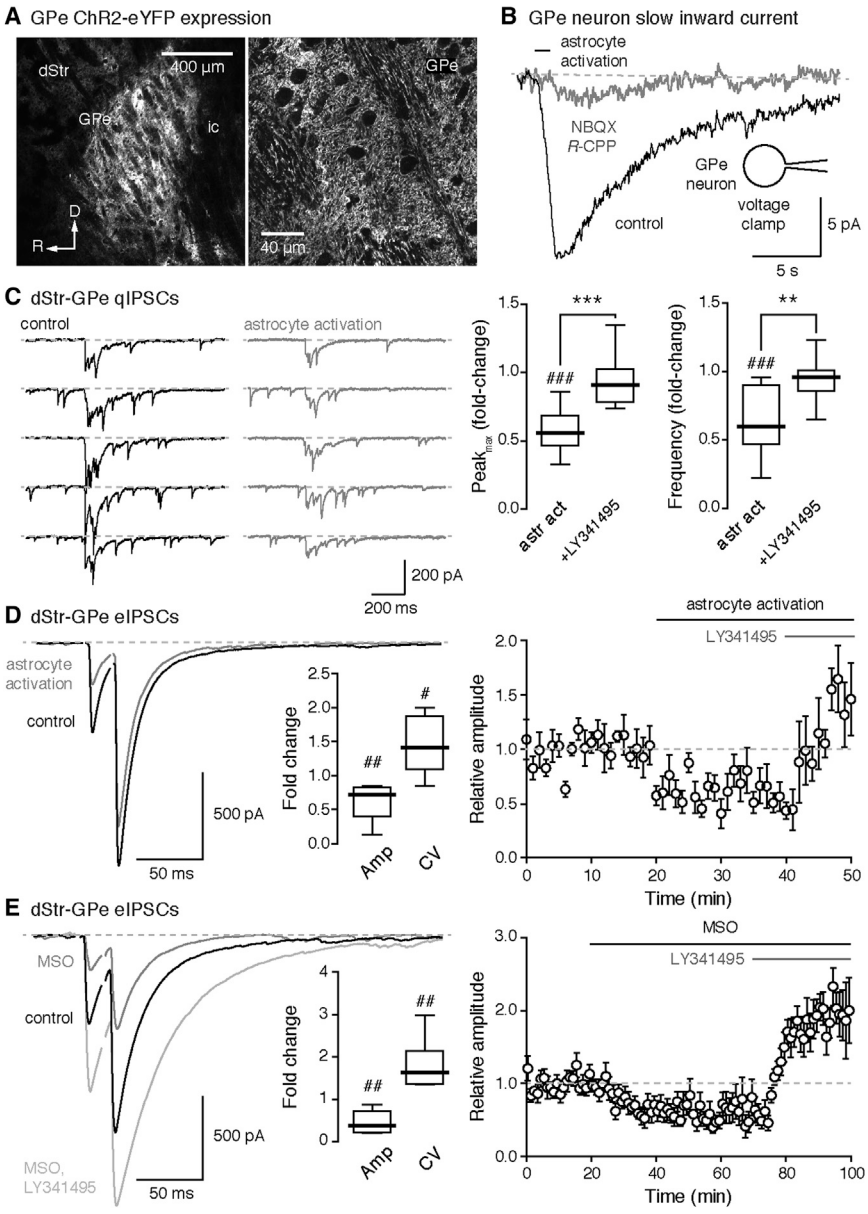

Figure 5. Astrocyte-Derived Glutamate Suppresses dStr-GPe GABA Release via Group II mGluRs

(A) Using $Gfap^{Cre}$ driver mouse, astrocyte-specific ChR2-eYFP expression was rendered with a genetic approach ($Gfap^{Cre}$;$R26^{LSL\text{-}ChR2(H314R)\text{-}eYFP}$). Left: confocal micrographs show ChR2-eYFP signal in a sagittal mouse brain section. Right: high-magnification image shows intense ChR2-eYFP signal in the GPe neuropil. dStr, dorsal striatum; ic, internal capsule.

(B) Optogenetic activation of astrocytes induced slow inward currents recorded in GPe neurons (n = 12 cells). These currents were sensitive to NMDA and AMPA receptor antagonists, *R*-CPP (20 μM) and NBQX (5 μM) (n = 7 cells).

(C) Left: representative dStr-GPe qIPSCs recorded in GPe neurons before (control) and during optogenetic astrocyte activation. Note the decrease in both maximal peak amplitude (n = 12 cells, p = 0.0005) and event frequency (n = 12 cells, p = 0.0005). LY341495 (200 nM) pre-incubation completely abolished this effect (maximal peak: n = 10 cells, p = 0.1934; frequency: n = 10 cells, p = 0.1602). The effect of astrocyte activation on dStr-GPe qIPSCs was reduced by LY341495 (maximal peak amplitude: p = 0.0004; frequency: p = 0.0033). This is summarized in a boxplot format (right).

(D) Left: representative dStr-GPe eIPSCs showing the effect of optogenetic astrocyte activation on dStr-GPe GABA release. Right: a population time course illustrates the stability of the recording and the consistency of the effect across cells. This effect was reversed by LY341495 (200 nM). Inset: boxplots summarize the effect of optogenetic astrocyte activation on dStr-GPe eIPSC amplitude (n = 8 cells, p = 0.0078) and CV (n = 8 cells, p = 0.0234).

(E) MSO (5 mM), a glutamine synthetase inhibitor, was bath applied to elevate intracellular glutamate content within astrocytes. Left: representative dStr-GPe eIPSCs show the effect of MSO on dStr-GPe GABA release. Right: a population time course illustrates the stability of the recording and the consistency of the effect across cells. This effect was reversed by LY341495 (200 nM). Inset: boxplots summarize the effect of MSO on dStr-GPe eIPSC amplitude (n = 8 cells, p = 0.0078) and CV (n = 8 cells, p = 0.0078).

Whiskers of the boxplots represent 10–90th percentiles. Means ± SEMs are presented for the time course plots.

II mGluRs. Optogenetic activation of the STN input reliably evoked ionotropic GluR-mediated EPSCs in all GPe neurons examined (n = 13 cells) (Figure 4G; Figure S3). In contrast, the same stimulation paradigm did not have a consistent effect on striatopallidal eIPSC amplitude (1.1 ± 0.5-fold, p = 0.5421) (Figure 4G).

Astrocyte-Derived Glutamate Activates Group II mGluRs at the Striatopallidal Terminals

Our data suggest a non-neuronal origin of ambient glutamate in ex vivo GPe tissue. In fact, the capacity for astrocytes to release glutamate is well described (Araque et al., 2014; Hamilton and Attwell, 2010; Haydon, 2001; Malarkey and Parpura, 2008; Newman, 2003; Theodosis et al., 2008; Volterra and Meldolesi, 2005). To directly demonstrate the capacity for GPe astrocytes to release glutamate, we expressed channelrhodopsin-2 (ChR2) in astrocytes (Gourine et al., 2010; Perea et al., 2014; Sasaki et al., 2012) using a $Gfap^{Cre}$ transgenic line (Figure 5A). Consistent with *Cre*-inducible tdTomato and GCaMP3 expression patterns (Figure 1), *Cre*-inducible ChR2 expression in the GPe was restricted to astrocytes (Figure S3). Optogenetic activation of GPe astrocytes excited neighboring

neurons, as evidenced by the increased firing and the corresponding slow inward currents (Figure 5B; Figure S3). These effects were sensitive to ionotropic glutamate receptor blockers NBQX (5 μM) and *R*-CPP (20 μM) (Figure 5B), but they were insensitive to TTX, SR95531, and picrotoxin (data not shown). These results confirmed that GPe astrocytes can indeed release glutamate.

We next examined if optogenetically evoked, astrocytic glutamate release could impact striatopallidal GABA transmission. To avoid confounding effects associated with the release of endocannabinoids (Navarrete and Araque, 2010), AM251 (a CB1 receptor antagonist, 2 μM) was included throughout the experiments. Under this condition, optogenetic activation of astrocytes reduced striatopallidal eIPSC amplitude (astrocyte activation = 0.7 ± 0.1-fold; p = 0.0078), accompanied by an increase in CV (control = 0.53 ± 0.13, astrocyte activation = 0.72 ± 0.22; p = 0.0234) (Figure 5D). Similarly, a decrease in striatopallidal quantal GABA release was observed in Sr^{2+}-containing external solution (Figure 5C). Group II mGluRs were crucial in mediating these effects, as preincubation of ex vivo slices in LY341495 completely blocked the ability of astrocyte activation to suppress GABA release (maximal peak = 0.9 ± 0.1-fold, p = 0.1934; frequency = 1.0 ± 0.1-fold, p = 0.1602) (Figure 5C). In contrast, the effect of optogenetic activation of astrocytes on striatopallidal eIPSC amplitude was not altered by the application of PSB36 (an adenosine A1 receptor antagonist, 10 nM) (naive = 0.7 ± 0.1-fold, n = 8 cells; PSB36 = 0.6 ± 0.2-fold, n = 7 cells; p = 0.7505). These findings corroborate those from experiments where no exogenous stimulus was applied, demonstrating that glutamate suppresses striatopallidal GABA release via the activation of group II mGluRs.

Given these results, inhibiting glutamine synthetase with methionine sulfoximine (MSO), which promotes astrocytic glutamate release by elevating cytosolic glutamate content (Tani et al., 2014), should inhibit striatopallidal GABA release. Consistent with our hypothesis, bath application of MSO (5 mM) decreased the striatopallidal eIPSC amplitude (MSO = 0.4 ± 0.2-fold; p = 0.0078) and increased the CV (control = 0.52 ± 0.15, MSO = 1.10 ± 0.33; p = 0.0078) (Figure 5E). The reduction in striatopallidal GABA release was not due to impaired synthesis and depletion of GABA, as LY341495 reversed the effect of MSO readily. Additionally, the effects of LY341495 on striatopallidal eIPSC amplitude were amplified in the presence of MSO (control = 2.3 ± 0.9-fold, MSO = 4.8 ± 1.8-fold; p = 0.0433), consistent with the elevated level of glutamate in ex vivo GPe tissue.

Chronic Dopamine Depletion Alters Astrocytic Gating of Striatopallidal Signaling

As we have shown that Ca^{2+} signaling is altered in GPe astrocytes following chronic 6-OHDA lesion, it raises the question of whether other key astrocytic functions, such as glutamate homeostasis, are altered in PD and whether altered astrocytic gating is responsible for increased striatopallidal GABA transmission in PD. To test the hypothesis that glutamate levels are altered in an in vivo setting, microdialysis was performed. As expected, dopamine levels in the GPe were greatly reduced in chronic 6-OHDA-lesioned animals. The extracellular glutamate content in the GPe was also decreased. In contrast, glutamine levels in the GPe were not altered (Figure S6).

If the decreased glutamate content in the GPe in vivo is a consequence of altered astrocytic function, we should be able to detect similar alterations in ex vivo brain slices. To investigate potential alterations in glutamate content ex vivo, patch-clamp recordings were performed to measure Ca^{2+}-mediated striatopallidal GABA release and its regulation by group II mGluRs. Following chronic 6-OHDA lesion, striatopallidal GABA release (as measured with eIPSC amplitude) was enhanced across a wide range of stimulation intensities (e.g., 500 μA: naive = 265.7 ± 126.6 pA, 6-OHDA = 653.7 ± 171.2 pA; p = 0.0410) (Figures 6A and 6B). Additionally, the increased striatopallidal GABA release was further indicated by decreases in both CV and paired-pulse ratio (Figure S5). The increased striatopallidal GABA release was attributable to reduced group II mGluR activity, as LY341495 had a diminished effect on striatopallidal eIPSC amplitude following chronic 6-OHDA lesion (e.g., 500 μA: 6-OHDA = 653.7 ± 171.2 pA, $6\text{-OHDA}_{LY341495}$ = 702.3 ± 505.5 pA; p = 0.6430) compared to that in naive mice (e.g., 500 μA: naive = 265.7 ± 126.6 pA, $\text{naive}_{LY341495}$ = 782.1 ± 324.2 pA; p = 0.0037). Importantly, LY341495 normalized the difference between naive and chronic 6-OHDA lesion condition in striatopallidal eIPSC amplitude (e.g., 500 μA: p = 0.4968) (Figures 6A and 6B). Furthermore, the difference in release probability was eliminated by LY341495, as measured with the CV and the paired-pulse ratio (Figure S5). A reduced effect with LY341495 was also observed on Sr^{2+}-mediated striatopallidal GABA release (Figure S5). The diminished effect with LY341495 was not due to a decreased mGluR3 expression, as demonstrated by the fluorescence-activated cell sorting (FACS)-qPCR analysis (Figure S4). Accordingly, LY379268 (a group II mGluR agonist) produced comparable effects on striatopallidal GABA release in both naive and 6-OHDA-lesioned mice (Figure S5).

To confirm that altered group II mGluR activity and striatopallidal GABA release indeed arises from chronic dopamine depletion rather than nonspecific effects of 6-OHDA, a *Cre-lox* strategy was used to abolish dopamine synthesis in nigral neurons in homozygous mice carrying the floxed tyrosine hydroxylase (*Th*) allele. Infection with Cre-AAV in the substantia nigra generated a conditional tyrosine hydroxylase knockout (Th-cKO), as evidenced by the loss of tyrosine hydroxylase at both nigral and striatal levels (Figures 6D and 6E). Similar to chronic 6-OHDA-lesioned mice, Th-cKO mice had a diminished LY341495 effect on striatopallidal GABA release compared to wild-type controls infected with a Cre-AAV (p = 0.0229) or floxed-Th mice infected with a GFP-AAV (p = 0.0496) (wild-type$^{\text{Cre-AAV}}$ = 2.1 ± 0.3-fold, $\text{Th}^{\text{fl/fl,GFP-AAV}}$ = 2.3 ± 0.2-fold, Th-cKO = 1.3 ± 0.1-fold). This observation is similar to the difference between naive and chronic 6-OHDA-lesioned mice ($\text{naive}_{LY341495}$ = 2.3 ± 0.9-fold, $6\text{-OHDA}_{LY341495}$ = 1.4 ± 0.3-fold; p = 0.0265) (Figure 6C). No difference between the two chronic dopamine depletion paradigms was observed (p = 0.9394) (Figure 6C). The magnitude of increase in striatopallidal GABA release by LY341495 was statistically indistinguishable between naive and wild-type infection control (p = 0.6254). These data argue that a disruption of group II mGluR-mediated

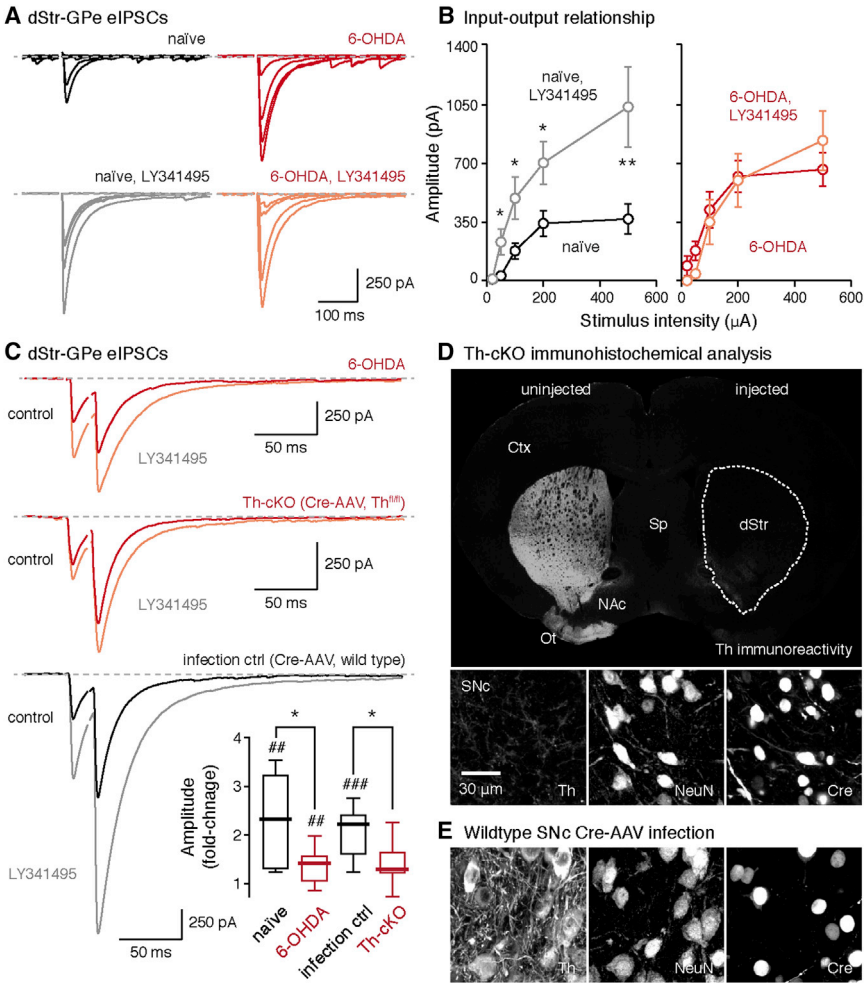

Figure 6. Increased dStr-GPe GABA Release following Chronic Dopamine Depletion Was due to a Decrease in mGluR-Mediated Suppression

(A) Representative dStr-GPe eIPSCs evoked with different stimulus intensities in various experimental conditions. Top: note the difference between naive mice (black) and chronic 6-OHDA-lesioned mice (red). Bottom: this difference was normalized by bath application of LY341495 (200 nM), a group II mGluR antagonist.

(B) Data summary showing the stimulus-response function of the dStr-GPe synapse with and without group II mGluR antagonism from naive mice (left) and chronic 6-OHDA-lesioned mice (right). LY341495 greatly increased the dStr-GPe eIPSC amplitude in naive mice (20 μA, $p = 0.5287$; 50 μA, $p = 0.0158$; 100 μA, $p = 0.0186$; 200 μA, $p = 0.0173$; 500 μA, $p = 0.0037$), but not in 6-OHDA-lesioned mice (20 μA, $p = 0.2348$; 50 μA, $p = 0.0929$; 100 μA, $p = 0.5345$; 200 μA, $p = 0.3882$; 500 μA, $p = 0.6430$). Means ± SEMs are presented.

(C) Top: representative eIPSCs showing a diminished effect of LY341495 on dStr-GPe GABA release in chronic 6-OHDA-lesioned mice. Middle: conditional tyrosine hydroxylase knockout (Th-cKO) mice were achieved with *Cre* delivery via an adeno-associated virus (Cre-AAV) in the substantia nigra pars compacta (SNc) of a homozygous floxed-*Th* ($Th^{fl/fl}$) mouse. LY341495 had an attenuated effect on dStr-GPe eIPSCs in this chronic dopamine depletion model. Bottom left: LY341495 displayed marked effect on dStr-GPe eIPSCs in wild-type mice with SNc Cre-AAV infection. Bottom right: boxplots summarize the effect of LY341495 on dStr-GPe eIPSCs in different experimental conditions (naive, n = 10 cells, $p = 0.0020$; 6-OHDA, n = 11 cells, $p = 0.0049$; infection control, n = 13 cells, $p = 0.0002$; Th-cKO, n = 9 cells, $p = 0.0742$). The effect of LY341495 was lower in chronic dopamine-depleted mice (naive versus 6-OHDA, $p = 0.0265$; infection control versus Th-cKO, $p = 0.0112$). No statistical significance between chronic 6-OHDA and Th-cKO was found ($p = 0.9394$). Similarly, no statistical significance between naive and infection control was found ($p = 0.4566$).

(D) Top: photomicrograph of a coronal brain section from a $Th^{fl/fl}$ mouse showing an overview of tyrosine hydroxylase immunoreactivity in the dStr and neighboring areas. Unilateral loss of tyrosine hydroxylase immunoreactivity in the dStr was observed in two mice with SNc Cre-AAV infection. Bottom: immunohistochemical analysis of the SNc from the same animal in the top panel is shown. Ctx, cortex; Sp, septum.

(E) Immunohistochemical analysis similar to that shown in (D) was performed on a wild-type mouse with Cre-AAV infection in the SNc as an infection control (infection ctrl).

Whiskers of the boxplots represent 10–90th percentiles.

regulation of striatopallidal GABA release was a consequence of chronic dopamine depletion rather than nonspecific toxic effects of 6-OHDA or viral infection.

The impact of intracellular Ca^{2+} on the expression and activity of transporters on the astrocytic membrane has been widely studied (Bazargani and Attwell, 2016). As we observed altered Ca^{2+} signaling in GPe astrocytes following chronic 6-OHDA lesion (Figures 1F and 1G), it is possible that decreased ambient glutamate levels were a consequence of increased astrocytic glutamate uptake. To this end, astrocytic glutamate transporter activity was measured with glutamate uncaging and whole-cell current-clamp recordings from SR101-labeled GPe astrocytes. The astrocytic identity was further confirmed by the ohmic current-voltage relationship (Figure 7A). Both whole-cell conductance (naive = 24.6 ± 12.8 nS, n = 25; 6-OHDA = 36.7 ± 16.6 nS, n = 15; $p = 0.5388$) and resting membrane potential (naive = −71.6 ± 3.9 mV, n = 35; 6-OHDA = −69.6 ± 2.5 mV, n = 30; $p = 0.0987$) of GPe astrocytes were unaltered following chronic 6-OHDA lesion (data not shown). Glutamate uncaging elicited depolarizing responses in GPe astrocytes (Figure 7B). These responses were blocked with *DL*-TBOA (100 μM), a glutamate transporter blocker (Figure S7). As ionotropic glutamate receptors and neuronal activity were blocked in these experiments (see the Supplemental Experimental Procedures), the release of neuroactive substances from local neurons and terminals upon glutamate uncaging was minimized. To our surprise, astrocytic glutamate transporter activity was decreased following chronic 6-OHDA lesion (naive = 2.7 ± 0.4 mV, 6-OHDA = 2.2 ± 0.2 mV; $p = 0.0017$) (Figure 7B).

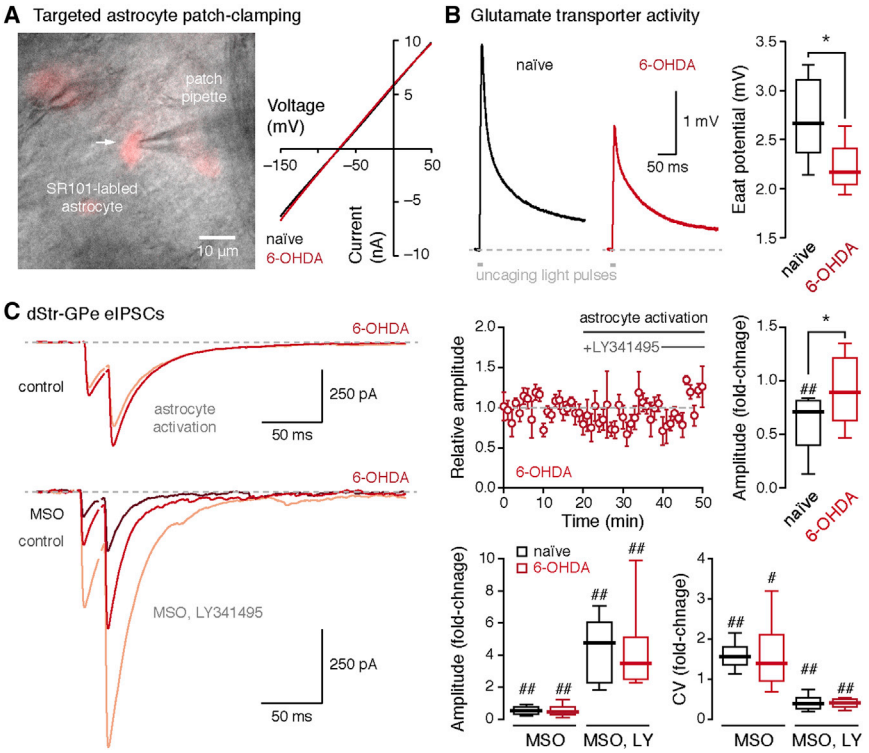

Figure 7. Astrocytic Regulation of dStr-GPe Release Was Disrupted following Chronic 6-OHDA Lesion

(A) Left: a composite micrograph of a GPe astrocyte (arrow). SR101 epifluorescence and differential interference contrast signals are shown. Right: representative recording shows currents in astrocytes elicited with a voltage ramp (from –150 to +50 mV) in naive (black) and 6-OHDA-lesioned (red) mice.

(B) Left: representative voltage records of glutamate transporter activity elicited with glutamate uncaging in astrocytes from naive (black) and 6-OHDA-lesioned (red) mice. Right: boxplots summarize the amplitude of glutamate transporter potential of astrocytes in naive (black) and 6-OHDA-lesioned (red) mice (naive, n = 13 cells; 6-OHDA, n = 15 cells; p = 0.0017).

(C) Top left: representative eIPSCs showing a lack of effect of optogenetic astrocyte activation in chronic 6-OHDA-lesioned mice. Top middle: average time course illustrates that optogenetic astrocyte activation did not alter dStr-GPe eIPSC amplitude. This was followed by LY341495 application to demonstrate that group II mGluRs at the dStr-GPe synapse were not near saturation in the 6-OHDA mice. Top right: boxplots summarize the effect of optogenetic astrocyte activation on dStr-GPe eIPSCs in naive and chronic 6-OHDA-lesioned mice (naive, n = 8 cells, p = 0.0078; 6-OHDA, n = 8 cells, p = 0.4609). A difference between the two conditions was observed (p = 0.0312). Bottom left: representative eIPSCs show the restoration of LY341495-induced enhancement on dStr-GPe GABA release in the presence of MSO in the chronic 6-OHDA-lesioned mice. Bottom middle: boxplots summarize the effect of LY341495 on dStr-GPe eIPSC amplitude following pretreatment with MSO (MSO: naive, n = 8 cells, p = 0.0078; 6-OHDA, n = 12 cells, p = 0.0024; LY341495 in MSO: naive, n = 10 cells, p = 0.0020; 6-OHDA, n = 8 cells, p = 0.0078). A comparable effect of LY341495 on dStr-GPe eIPSC amplitude was found in naive and 6-OHDA-lesioned mice in the presence of MSO (p = 0.8968). Bottom right: boxplots summarize the effect of LY341495 on dStr-GPe eIPSC CV following pretreatment with MSO (MSO: naive, n = 8 cells, p = 0.0078; 6-OHDA, n = 12 cells, p = 0.0342; LY341495 in MSO: naive, n = 10 cells, p = 0.0020; 6-OHDA, n = 8 cells, p = 0.0078). A comparable effect of LY341495 on dStr-GPe eIPSC CV was found in naive and 6-OHDA-lesioned mice in the presence of MSO (p = 0.8868).

Whiskers of the boxplots represent 10–90th percentiles. Means ± SEMs are presented for the time course plots.

We hypothesized that the diminished ambient glutamate levels in the GPe tissue following chronic dopamine depletion arose from an impaired astrocytic glutamate release. As optogenetic activation of GPe astrocytes reliably induced glutamate release, similar experiments were repeated in chronic 6-OHDA-lesioned mice. In contrast with observations in naive mice, optogenetic activation of GPe astrocytes did not induce changes in striatopallidal eIPSCs in 6-OHDA-lesioned mice (astrocyte activation = 0.9 ± 0.3-fold, p = 0.4609) (Figure 7C). If GPe astrocytes have a diminished intracellular content of glutamate, then blocking its conversion to glutamine should restore glutamate release in chronic 6-OHDA-lesioned mice. Consistent with this hypothesis, MSO inhibited striatopallidal GABA release in 6-OHDA-lesioned mice as measured by eIPSC amplitude (MSO = 0.4 ± 0.2-fold, p = 0.0024) and CV (MSO = 1.4 ± 0.6-fold, p = 0.0342) (Figure 7C). LY341495 produced comparable effects in naive and 6-OHDA conditions following the preincubation of MSO, as measured with eIPSC amplitude (naive = 4.8 ± 1.8-fold, 6-OHDA = 3.5 ± 1.0-fold; p = 0.8968) and CV (naive = 0.4 ± 0.1-fold, 6-OHDA = 0.4 ± 0.1-fold; p = 0.8868) (Figure 7C). These data indicate that reduced astrocytic glutamate content contributes to the low ambient glutamate level and elevated striatopallidal GABA release in the chronic 6-OHDA-lesioned mice.

DISCUSSION

Despite the importance of astrocytes in the maintenance of proper neuronal function, only a handful of studies address the roles of astrocytes in basal ganglia function in normal brain states and dysfunction in PD. The classic circuit model predicts an increased output of dStr indirect pathway projection neurons in the absence of dopamine (Albin et al., 1989; DeLong, 1990). In this study, we provided direct evidence for the increased striatopallidal release following the chronic loss of dopamine, and we illuminated the contributions from GPe astrocytes.

Astrocytes Are Integral Parts of the Striatopallidal System

While interactions between astrocytes and excitatory synapses have been examined extensively, our findings argue that GPe astrocytes play an integral role at the GABAergic striatopallidal synapse, which should be considered a tripartite synapse. In addition to the supporting roles of GPe astrocytes (via clearance and re-uptake of substrates) at the striatopallidal synapse

(Galvan et al., 2010), our data suggest that GPe astrocytes are active partners in shaping the strength of the striatopallidal inputs. Specifically, by controlling extracellular glutamate levels via the release and uptake process, GPe astrocytes suppress striatopallidal release via presynaptic group II mGluRs.

We found that astrocytic control of glutamate homeostasis in the GPe is responsive to chronic 6-OHDA lesion. The lower ambient glutamate levels in the GPe tissue milieu following chronic loss of dopamine led to a disinhibition of striatopallidal input as a result of decreased group II mGluR activation. Importantly, boosting astrocytic glutamate content restored tonic mGluR activity in the chronic 6-OHDA-lesioned mice. Our findings are consistent with the literature that astrocytes are involved in the maintenance of ambient glutamate, and this process is altered in disease conditions (Cavelier et al., 2005; Featherstone and Shippy, 2008; Halassa et al., 2007; Kalivas, 2009; Maragakis and Rothstein, 2006; Sofroniew and Vinters, 2010).

Glutamate Content Is Highly Compartmentalized

Unlike gliotransmission reported in the majority of the studies (Araque et al., 2014), ambient glutamate levels in ex vivo GPe tissue were observed in the absence of external stimuli or pharmacological manipulations. Tonic activation of presynaptic mGluRs has been observed previously (Forsythe and Clements, 1990; Losonczy et al., 2003; McBain et al., 1994). Tonic activation of postsynaptic NMDA receptors in the hippocampus (Le Meur et al., 2007), thalamus (Crabtree et al., 2013), and cerebellum has also been observed (Huang and Bordey, 2004). These results demonstrate the presence of ambient glutamate maintained in ex vivo tissue. Our current study extends the idea that ambient glutamate is present in ex vivo GPe tissue.

It is conceivable that glutamate concentration is highly cell compartment specific. While ambient glutamate in the GPe can establish a steady-state desensitization of glutamate receptors, especially AMPA receptors (Dingledine et al., 1999), glutamate concentrations likely vary widely across cellular subcompartments, leaving AMPA receptors in the GPe functionally intact. As group II mGluRs at the striatopallidal synapse are tonically active, local glutamate levels at the striatopallidal synapses can be in the submicromolar range based on the affinity of these receptors to glutamate (Schoepp et al., 1999). In contrast, group III mGluRs that are present at striatopallidal synapses and exhibit micromolar affinity for glutamate are not tonically active (Macinnes and Duty, 2008; Matsui and Kita, 2003; Valenti et al., 2003).

The Origin of Ambient Glutamate in the GPe

To address the origin of ambient glutamate levels observed in the ex vivo GPe tissue, we first excluded the contribution from the principal glutamatergic input to the GPe (i.e., the STN) by showing that (1) silencing the STN input did not alter ambient glutamate levels and (2) direct stimulation of the STN-GPe input similarly did not modulate striatopallidal GABA release. Using optogenetic and pharmacological manipulations, we show that GPe astrocytes have the capacity to elevate extracellular glutamate content in ex vivo GPe tissue. These data argue that astrocytic release of glutamate can contribute to ambient glutamate levels in the GPe tissue. However, whether GPe astrocytes are the sole source of glutamate that is maintained in the GPe tissue ex vivo requires further investigation. Importantly, we found that elevation of astrocytic glutamate content restores glutamate-mediated control of striatopallidal GABA release following chronic 6-OHDA lesion. We argue that disruption of intracellular glutamate homeostasis within GPe astrocytes contributes to alterations in tissue-level glutamate content and, subsequently, to alterations in circuit-level dysfunction in PD. Our study extends the literature on impaired astrocytic functions as a common feature of neurodegenerative diseases (Halassa et al., 2007; Lobsiger and Cleveland, 2007; Maragakis and Rothstein, 2006; Sofroniew and Vinters, 2010).

Neuronal Influence on Glutamate Homeostasis in GPe Astrocytes

The high levels of ambient glutamate in the GPe are not because of poor uptake efficiency as a result of a low astrocyte density. Instead, we found that the astrocyte-to-neuron ratio in the GPe is roughly two-to-one, an order of magnitude higher than that in the dStr. In contrast, we speculate that, as the maintenance of the relatively high levels of glutamate in the GPe can be energetically expensive, the high density of astrocytes within the GPe should lessen the energetic burden on individual astrocytes. Additionally, astrocyte number appears to correlate with the high activity levels of GPe neurons both ex vivo and in vivo (Hegeman et al., 2016; Jaeger and Kita, 2011) and, thus, their high metabolic demand (Harris et al., 2012). This idea is further supported by the high astrocyte-to-neuron ratio established by Purkinje neurons and Bergmann glial cells in the cerebellum (Lafarga et al., 1993). On the contrary, the astrocyte-neuron ratio in the rodent cortex, which is metabolically less active, is one to three (Nedergaard et al., 2003).

Biological Importance of Astrocytic Gating of Striatopallidal Input

GPe astrocytes gate striatopallidal input via control of ambient glutamate. This modulatory control increases the dynamic range of the striatopallidal input and filters out unwanted, weak signals. This process could be important for encoding functional segregation of movements within the GPe (Hegeman et al., 2016; Jin et al., 2014; Shi et al., 2004; Turner and Anderson, 2005). The pathophysiology of PD can be explained by the changes in the activity levels and synchrony in the GPe (Bergman et al., 1998; Chan et al., 2011; Hegeman et al., 2016; Hernández et al., 2015; Kita and Kita, 2011). In a normal state, individual GPe neurons respond specifically to the movement in one direction of a single joint on the contralateral side. On the contrary, individual GPe neurons in PD respond to movements of multiple joints and body parts (Filion et al., 1988). As dopamine is considered to be pivotal in isolating information related to movements of specific body parts (Bergman et al., 1998), it is intriguing to speculate that the crosstalk of information related to different body parts in the absence of dopamine in part arises from the disinhibition of striatopallidal GABA transmission as a consequence of altered glutamate homeostasis. Accordingly, restoring glutamate homeostasis in the GPe should suppress striatopallidal GABA transmission and ameliorate motor symptoms of PD.

EXPERIMENTAL PROCEDURES

All experiments detailed are in accord with the Northwestern University Animal Care and Use Committee, the University of Michigan Unit for Laboratory Animal Medicine, and are in compliance with the NIH Guide for the Care and Use of Laboratory Animals. All mice were on a C57BL/6 background. Unilateral lesion of the nigrostriatal system was produced by 6-hydroxydopamine HCl injection into the medial forebrain bundle of adult mice (postnatal days 28–35). To genetically abolish nigral dopamine release, CMV-GFP-Cre AAV injections were targeted to the substantia nigra pars compacta of homozygous floxed-Th mice. For detection of glutamate in ex vivo slices, GFAP-iGluSnFr AAV was injected into wild-type mice. For astrocyte-specific optogenetic activation, a $Gfap^{Cre}$ mouse line was crossed with $R26^{LSL\text{-}hChR2(H134R)\text{-}eYFP}$ mouse line to obtain astrocyte-specific expression of ChR2. Alternatively, EF1α-CreOn-hChR2(H134R)-eYFP AAV was injected into the GPe of $Gfap^{Cre}$ mice. For STN-specific optogenetic activation, hSyn-hChR2(H134R)-eYFP AAV was injected into the STN of wild-type mice. To abolish STN glutamate release, a tetanus toxin light chain (CMV-TeTLC-2A-eGFP)-expressing AAV was injected into the STN of wild-type mice; alternatively, CMV-eGFP-Cre AAV was injected into the STN of homozygous floxed-VGluT2 mice.

Mice at postnatal days 55–75 were used for ex vivo experiments. SR101 was used to label astrocytes. To study the dStr inputs to the GPe, striatopallidal axons were stimulated within the dStr using an electrical stimulus. To activate ChR2 in astrocytes, a 1- to 2-s period of sustained blue light or pulsed blue light (50 ms each at 10 Hz) was used. For GCaMP3 and iGluSnFR imaging, standard brain slices were prepared. Signals were acquired with a 60 × 1.0 numerical aperture (NA) water-immersion objective, spinning-disk unit, and an electron-multiplying charge-coupled device (CCD). Standard procedures were used for immunohistochemistry. Immunoreactivity was examined on a laser-scanning confocal microscope with a 60 × 1.35 NA oil-immersion objective.

Data analyses were done with ClampFit10, MiniAnalysis, IgorPro6, MATLAB8, Fiji, and Python3. Data in the main text are presented as median values ± median absolute deviations as a measure of central tendency and statistical dispersion, respectively. Boxplots were used for graphic representation. Mann-Whitney *U* test, Wilcoxon signed-rank test, and Fisher's exact test were used.

SUPPLEMENTAL INFORMATION

Supplemental Information includes Supplemental Experimental Procedures, seven figures, and two tables and can be found with this article online at http://dx.doi.org/10.1016/j.celrep.2016.10.087.

AUTHOR CONTRIBUTIONS

Q.C. conceived the study. Q.C., J.E.P., and A.P. designed, conducted, and analyzed the electrophysiological and optical measurements. Q.C., J.E.P., A.P., and M.P.F. performed the immunohistochemical experiments. J.E.P., A.P., and I.B.F. performed the morphometric analyses. Q.C. collected cells with FACS. E.C.A. conducted the qPCR experiments. M.P.F. and K.A.Y. provided technical support and performed pilot/validation studies. J.-F.P. and R.A. generated the floxed-tyrosine hydroxylase mouse line. O.S.M. and R.T.K. performed in vivo microdialysis. Q.C., J.E.P., and C.S.C. wrote the manuscript. All authors reviewed and edited the manuscript. C.S.C. directed and supervised the project.

ACKNOWLEDGMENTS

We would like to thank Tina Huang, Daniel Kelver, and Bonnie Erjavec for their technical assistance; Dr. Loren Looger for sharing the iGluSnFR construct and the helpful dialogue; and Dr. Tracy Gertler and members of the C.S.C. lab for discussion. This work was supported by grants to J.E.P. (NIH grants AG020506 and AG047782), A.P. (NIH grant AG020506), O.S.M. (Michigan Institute for Clinical and Health Research grant 2UL1TR000433), R.T.K. (NIH grant EB003320), R.A. (Northwestern Memorial Foundation and NIH grants NS072703 and NS071081), and C.S.C. (a Bachmann-Strauss grant, a DoD contract W81XWH-13-1-0243, and NIH grants NS069777 and NS047085).

Received: April 1, 2016
Revised: September 7, 2016
Accepted: October 27, 2016
Published: November 22, 2016

REFERENCES

Agulhon, C., Petravicz, J., McMullen, A.B., Sweger, E.J., Minton, S.K., Taves, S.R., Casper, K.B., Fiacco, T.A., and McCarthy, K.D. (2008). What is the role of astrocyte calcium in neurophysiology? Neuron *59*, 932–946.

Albin, R.L., Young, A.B., and Penney, J.B. (1989). The functional anatomy of basal ganglia disorders. Trends Neurosci. *12*, 366–375.

Araque, A., Carmignoto, G., Haydon, P.G., Oliet, S.H., Robitaille, R., and Volterra, A. (2014). Gliotransmitters travel in time and space. Neuron *81*, 728–739.

Bazargani, N., and Attwell, D. (2016). Astrocyte calcium signaling: the third wave. Nat. Neurosci. *19*, 182–189.

Benediktsson, A.M., Marrs, G.S., Tu, J.C., Worley, P.F., Rothstein, J.D., Bergles, D.E., and Dailey, M.E. (2012). Neuronal activity regulates glutamate transporter dynamics in developing astrocytes. Glia *60*, 175–188.

Bergman, H., Feingold, A., Nini, A., Raz, A., Slovin, H., Abeles, M., and Vaadia, E. (1998). Physiological aspects of information processing in the basal ganglia of normal and parkinsonian primates. Trends Neurosci. *21*, 32–38.

Cavelier, P., Hamann, M., Rossi, D., Mobbs, P., and Attwell, D. (2005). Tonic excitation and inhibition of neurons: ambient transmitter sources and computational consequences. Prog. Biophys. Mol. Biol. *87*, 3–16.

Chan, C.S., Glajch, K.E., Gertler, T.S., Guzman, J.N., Mercer, J.N., Lewis, A.S., Goldberg, A.B., Tkatch, T., Shigemoto, R., Fleming, S.M., et al. (2011). HCN channelopathy in external globus pallidus neurons in models of Parkinson's disease. Nat. Neurosci. *14*, 85–92.

Crabtree, J.W., Lodge, D., Bashir, Z.I., and Isaac, J.T. (2013). GABAA, NMDA and mGlu2 receptors tonically regulate inhibition and excitation in the thalamic reticular nucleus. Eur. J. Neurosci. *37*, 850–859.

Del Castillo, J., and Katz, B. (1954). Quantal components of the end-plate potential. J. Physiol. *124*, 560–573.

DeLong, M.R. (1990). Primate models of movement disorders of basal ganglia origin. Trends Neurosci. *13*, 281–285.

Dingledine, R., Borges, K., Bowie, D., and Traynelis, S.F. (1999). The glutamate receptor ion channels. Pharmacol. Rev. *51*, 7–61.

Featherstone, D.E., and Shippy, S.A. (2008). Regulation of synaptic transmission by ambient extracellular glutamate. Neuroscientist *14*, 171–181.

Filion, M., Tremblay, L., and Bédard, P.J. (1988). Abnormal influences of passive limb movement on the activity of globus pallidus neurons in parkinsonian monkeys. Brain Res. *444*, 165–176.

Forsythe, I.D., and Clements, J.D. (1990). Presynaptic glutamate receptors depress excitatory monosynaptic transmission between mouse hippocampal neurones. J. Physiol. *429*, 1–16.

Galvan, A., Hu, X., Smith, Y., and Wichmann, T. (2010). Localization and function of GABA transporters in the globus pallidus of parkinsonian monkeys. Exp. Neurol. *223*, 505–515.

Gourine, A.V., Kasymov, V., Marina, N., Tang, F., Figueiredo, M.F., Lane, S., Teschemacher, A.G., Spyer, K.M., Deisseroth, K., and Kasparov, S. (2010). Astrocytes control breathing through pH-dependent release of ATP. Science *329*, 571–575.

Halassa, M.M., Fellin, T., and Haydon, P.G. (2007). The tripartite synapse: roles for gliotransmission in health and disease. Trends Mol. Med. *13*, 54–63.

Hamilton, N.B., and Attwell, D. (2010). Do astrocytes really exocytose neurotransmitters? Nat. Rev. Neurosci. *11*, 227–238.

Harris, J.J., Jolivet, R., and Attwell, D. (2012). Synaptic energy use and supply. Neuron *75*, 762–777.

Haydon, P.G. (2001). GLIA: listening and talking to the synapse. Nat. Rev. Neurosci. *2*, 185–193.

Hegeman, D.J., Hong, E.S., Hernández, V.M., and Chan, C.S. (2016). The external globus pallidus: progress and perspectives. Eur. J. Neurosci. *43*, 1239–1265.

Hernández, V.M., Hegeman, D.J., Cui, Q., Kelver, D.A., Fiske, M.P., Glajch, K.E., Pitt, J.E., Huang, T.Y., Justice, N.J., and Chan, C.S. (2015). Parvalbumin+ neurons and Npas1+ neurons are distinct neuron classes in the mouse external globus pallidus. J. Neurosci. *35*, 11830–11847.

Hornykiewicz, O. (1998). Biochemical aspects of Parkinson's disease. Neurology *51* (*2, Suppl 2*), S2–S9.

Huang, H., and Bordey, A. (2004). Glial glutamate transporters limit spillover activation of presynaptic NMDA receptors and influence synaptic inhibition of Purkinje neurons. J. Neurosci. *24*, 5659–5669.

Jaeger, D., and Kita, H. (2011). Functional connectivity and integrative properties of globus pallidus neurons. Neuroscience *198*, 44–53.

Jin, X., Tecuapetla, F., and Costa, R.M. (2014). Basal ganglia subcircuits distinctively encode the parsing and concatenation of action sequences. Nat. Neurosci. *17*, 423–430.

Kalivas, P.W. (2009). The glutamate homeostasis hypothesis of addiction. Nat. Rev. Neurosci. *10*, 561–572.

Khakh, B.S., and Sofroniew, M.V. (2015). Diversity of astrocyte functions and phenotypes in neural circuits. Nat. Neurosci. *18*, 942–952.

Kita, H., and Kita, T. (2011). Role of striatum in the pause and burst generation in the globus pallidus of 6-OHDA-treated rats. Front. Syst. Neurosci. *5*, 42.

Kravitz, A.V., Freeze, B.S., Parker, P.R., Kay, K., Thwin, M.T., Deisseroth, K., and Kreitzer, A.C. (2010). Regulation of parkinsonian motor behaviours by optogenetic control of basal ganglia circuitry. Nature *466*, 622–626.

Lafarga, M., Berciano, M.T., Saurez, I., Andres, M.A., and Berciano, J. (1993). Reactive astroglia-neuron relationships in the human cerebellar cortex: a quantitative, morphological and immunocytochemical study in Creutzfeldt-Jakob disease. Int. J. Dev. Neurosci. *11*, 199–213.

Lange, H., Thörner, G., Hopf, A., and Schröder, K.F. (1976). Morphometric studies of the neuropathological changes in choreatic diseases. J. Neurol. Sci. *28*, 401–425.

Le Meur, K., Galante, M., Angulo, M.C., and Audinat, E. (2007). Tonic activation of NMDA receptors by ambient glutamate of non-synaptic origin in the rat hippocampus. J. Physiol. *580*, 373–383.

Lemos, J.C., Friend, D.M., Kaplan, A.R., Shin, J.H., Rubinstein, M., Kravitz, A.V., and Alvarez, V.A. (2016). Enhanced GABA transmission drives bradykinesia following loss of dopamine D2 receptor signaling. Neuron *90*, 824–838.

Lobsiger, C.S., and Cleveland, D.W. (2007). Glial cells as intrinsic components of non-cell-autonomous neurodegenerative disease. Nat. Neurosci. *10*, 1355–1360.

Losonczy, A., Somogyi, P., and Nusser, Z. (2003). Reduction of excitatory postsynaptic responses by persistently active metabotropic glutamate receptors in the hippocampus. J. Neurophysiol. *89*, 1910–1919.

Macinnes, N., and Duty, S. (2008). Group III metabotropic glutamate receptors act as hetero-receptors modulating evoked GABA release in the globus pallidus in vivo. Eur. J. Pharmacol. *580*, 95–99.

Malarkey, E.B., and Parpura, V. (2008). Mechanisms of glutamate release from astrocytes. Neurochem. Int. *52*, 142–154.

Malinow, R., and Tsien, R.W. (1990). Presynaptic enhancement shown by whole-cell recordings of long-term potentiation in hippocampal slices. Nature *346*, 177–180.

Maragakis, N.J., and Rothstein, J.D. (2006). Mechanisms of disease: astrocytes in neurodegenerative disease. Nat. Clin. Pract. Neurol. *2*, 679–689.

Martín, R., Bajo-Grañeras, R., Moratalla, R., Perea, G., and Araque, A. (2015). Circuit-specific signaling in astrocyte-neuron networks in basal ganglia pathways. Science *349*, 730–734.

Marvin, J.S., Borghuis, B.G., Tian, L., Cichon, J., Harnett, M.T., Akerboom, J., Gordus, A., Renninger, S.L., Chen, T.W., Bargmann, C.I., et al. (2013). An optimized fluorescent probe for visualizing glutamate neurotransmission. Nat. Methods *10*, 162–170.

Matsui, T., and Kita, H. (2003). Activation of group III metabotropic glutamate receptors presynaptically reduces both GABAergic and glutamatergic transmission in the rat globus pallidus. Neuroscience *122*, 727–737.

McBain, C.J., DiChiara, T.J., and Kauer, J.A. (1994). Activation of metabotropic glutamate receptors differentially affects two classes of hippocampal interneurons and potentiates excitatory synaptic transmission. J. Neurosci. *14*, 4433–4445.

Middeldorp, J., and Hol, E.M. (2011). GFAP in health and disease. Prog. Neurobiol. *93*, 421–443.

Minelli, A., Barbaresi, P., Reimer, R.J., Edwards, R.H., and Conti, F. (2001). The glial glutamate transporter GLT-1 is localized both in the vicinity of and at distance from axon terminals in the rat cerebral cortex. Neuroscience *108*, 51–59.

Navarrete, M., and Araque, A. (2010). Endocannabinoids potentiate synaptic transmission through stimulation of astrocytes. Neuron *68*, 113–126.

Nedergaard, M., Ransom, B., and Goldman, S.A. (2003). New roles for astrocytes: redefining the functional architecture of the brain. Trends Neurosci. *26*, 523–530.

Nedergaard, M., Rodríguez, J.J., and Verkhratsky, A. (2010). Glial calcium and diseases of the nervous system. Cell Calcium *47*, 140–149.

Newman, E.A. (2003). New roles for astrocytes: regulation of synaptic transmission. Trends Neurosci. *26*, 536–542.

Nimmerjahn, A., Kirchhoff, F., Kerr, J.N., and Helmchen, F. (2004). Sulforhodamine 101 as a specific marker of astroglia in the neocortex in vivo. Nat. Methods *1*, 31–37.

Ohishi, H., Shigemoto, R., Nakanishi, S., and Mizuno, N. (1993). Distribution of the mRNA for a metabotropic glutamate receptor (mGluR3) in the rat brain: an in situ hybridization study. J. Comp. Neurol. *335*, 252–266.

Perea, G., and Araque, A. (2005). Glial calcium signaling and neuron-glia communication. Cell Calcium *38*, 375–382.

Perea, G., Navarrete, M., and Araque, A. (2009). Tripartite synapses: astrocytes process and control synaptic information. Trends Neurosci. *32*, 421–431.

Perea, G., Yang, A., Boyden, E.S., and Sur, M. (2014). Optogenetic astrocyte activation modulates response selectivity of visual cortex neurons in vivo. Nat. Commun. *5*, 3262.

Salvesen, L., Ullerup, B.H., Sunay, F.B., Brudek, T., Løkkegaard, A., Agander, T.K., Winge, K., and Pakkenberg, B. (2015). Changes in total cell numbers of the basal ganglia in patients with multiple system atrophy - A stereological study. Neurobiol. Dis. *74*, 104–113.

Sasaki, T., Beppu, K., Tanaka, K.F., Fukazawa, Y., Shigemoto, R., and Matsui, K. (2012). Application of an optogenetic byway for perturbing neuronal activity via glial photostimulation. Proc. Natl. Acad. Sci. USA *109*, 20720–20725.

Schoepp, D.D., Jane, D.E., and Monn, J.A. (1999). Pharmacological agents acting at subtypes of metabotropic glutamate receptors. Neuropharmacology *38*, 1431–1476.

Shi, L.H., Luo, F., Woodward, D.J., and Chang, J.Y. (2004). Neural responses in multiple basal ganglia regions during spontaneous and treadmill locomotion tasks in rats. Exp. Brain Res. *157*, 303–314.

Shigetomi, E., Patel, S., and Khakh, B.S. (2016). Probing the complexities of astrocyte calcium signaling. Trends Cell Biol. *26*, 300–312.

Shink, E., and Smith, Y. (1995). Differential synaptic innervation of neurons in the internal and external segments of the globus pallidus by the GABA- and glutamate-containing terminals in the squirrel monkey. J. Comp. Neurol. *358*, 119–141.

Sofroniew, M.V., and Vinters, H.V. (2010). Astrocytes: biology and pathology. Acta Neuropathol. *119*, 7–35.

Tanabe, Y., Nomura, A., Masu, M., Shigemoto, R., Mizuno, N., and Nakanishi, S. (1993). Signal transduction, pharmacological properties, and expression patterns of two rat metabotropic glutamate receptors, mGluR3 and mGluR4. J. Neurosci. *13*, 1372–1378.

Tani, H., Dulla, C.G., Farzampour, Z., Taylor-Weiner, A., Huguenard, J.R., and Reimer, R.J. (2014). A local glutamate-glutamine cycle sustains synaptic excitatory transmitter release. Neuron *81*, 888–900.

Tepper, J.M., Abercrombie, E.D., and Bolam, J.P. (2007). Basal ganglia macrocircuits. Prog. Brain Res. *160*, 3–7.

Testa, C.M., Standaert, D.G., Young, A.B., and Penney, J.B., Jr. (1994). Metabotropic glutamate receptor mRNA expression in the basal ganglia of the rat. J. Neurosci. *14*, 3005–3018.

Theodosis, D.T., Poulain, D.A., and Oliet, S.H. (2008). Activity-dependent structural and functional plasticity of astrocyte-neuron interactions. Physiol. Rev. *88*, 983–1008.

Tong, X., Ao, Y., Faas, G.C., Nwaobi, S.E., Xu, J., Haustein, M.D., Anderson, M.A., Mody, I., Olsen, M.L., Sofroniew, M.V., and Khakh, B.S. (2014). Astrocyte Kir4.1 ion channel deficits contribute to neuronal dysfunction in Huntington's disease model mice. Nat. Neurosci. *17*, 694–703.

Traynelis, S.F., Wollmuth, L.P., McBain, C.J., Menniti, F.S., Vance, K.M., Ogden, K.K., Hansen, K.B., Yuan, H., Myers, S.J., and Dingledine, R. (2010). Glutamate receptor ion channels: structure, regulation, and function. Pharmacol. Rev. *62*, 405–496.

Turner, R.S., and Anderson, M.E. (2005). Context-dependent modulation of movement-related discharge in the primate globus pallidus. J. Neurosci. *25*, 2965–2976.

Tzingounis, A.V., and Wadiche, J.I. (2007). Glutamate transporters: confining runaway excitation by shaping synaptic transmission. Nat. Rev. Neurosci. *8*, 935–947.

Valenti, O., Marino, M.J., Wittmann, M., Lis, E., DiLella, A.G., Kinney, G.G., and Conn, P.J. (2003). Group III metabotropic glutamate receptor-mediated modulation of the striatopallidal synapse. J. Neurosci. *23*, 7218–7226.

Volterra, A., and Meldolesi, J. (2005). Astrocytes, from brain glue to communication elements: the revolution continues. Nat. Rev. Neurosci. *6*, 626–640.

Wichmann, T., and DeLong, M.R. (1996). Functional and pathophysiological models of the basal ganglia. Curr. Opin. Neurobiol. *6*, 751–758.